Efficient formation, isolation and characterization of poly(3-alkylthiophene) nanofibres: probing order as a function of side-chain length

Peer-reviewed author version

OOSTERBAAN, Wibren; VRINDTS, Veerle; RUTTENS, Bart; Berson, Solenn; Guillerez, Stephane; DOUHERET, Olivier; D'HAEN, Jan; ADRIAENSENS, Peter; MANCA, Jean; LUTSEN, Laurence & VANDERZANDE, Dirk (2009) Efficient formation, isolation and characterization of poly(3-alkylthiophene) nanofibres: probing order as a function of side-chain length. In: JOURNAL OF MATERIALS CHEMISTRY, 19(30). p. 5424-5435.

DOI: 10.1039/b900670b
Handle: http://hdl.handle.net/1942/9831

Efficient formation, isolation and characterization of poly(3-alkylthiophene) nanofibres: probing order as a function of side-chain length

Wibren D. Oosterbaan,[†] *Veerle Vrindts,*[§] *Solenn Berson,*[‡] *Stéphane Guillerez,*[‡] *Olivier Douhéret,*[§] *Bart Ruttens,*[§] *Jan D'Haen,*[†] *Peter Adriaensens,*[†] *Jean Manca,*[†,§] *Laurence Lutsen,*[§] *Dirk Vanderzande*[†,§,*]

[†] Hasselt University, Campus Diepenbeek, Institute for Materials Research, Agoralaan Building D, 3590 Diepenbeek, Belgium, and [‡] CEA Grenoble INAC/SPrAM, INES-RDI, 17 rue des martyrs, 38054 Grenoble cedex 09, France, and [§] IMEC-IMOMEC, Wetenschapspark 1, 3590 Diepenbeek, Belgium.

* Corresponding author: dirk.vanderzande@uhasselt.be

[†] Hasselt University.

[‡] CEA.

[§] IMEC-IMOMEC.

Summary

Efficient fibre formation for all regioregular poly(3-alkylthiophene)s (P3*A*Ts) with alkyl chain lengths (*A*) between 3 and 9 carbon atoms has been accomplished in several solvents. It was observed that for the aliphatic and (chlorinated) aromatic hydrocarbon solvents used, the solvent refractive index offers some rationale to predict the feasibility of a solvent for fibre formation. The fibres were separated from remaining non-organised polymer by centrifugation. This enabled the characterisation of the isolated fibres in function of alkyl chain length (*A*) with TEM, AFM, XRD and UV-Vis spectroscopy. The fibres are 20 +/− 5 nm wide and 0.5 to >4 μm long and mainly crystallize in the common type I crystal phase. The order within the fibres was probed with XRD, SAED, and UV-Vis and was found to strongly improve with increasing alkyl chain length in going from P33T to P35T, resulting in a longer conjugation length. For P35T to P39T the improvement in order is only marginal.

Fibres from P37T, were found to mainly crystallize in a crystal phase slightly different from type I that we refer to as type I'. This new crystal structure has a lattice constant *a* that is marginally shorter than that of phase I and a slightly longer lattice constant *b* of 4.0 Å and thus in XRD can hardly be distinguished from phase I. It is furthermore characterized by a blue-shifted absorption band in UV-Vis spectroscopy. The type I' fibres were converted in normal type I fibres in the solid state at 70 °C and in solution around 50 °C.

1. Introduction

Regioregular poly(3-alkylthiophene)s (P3*A*Ts) are among the most widely studied conjugated polymers for organic electronic devices. Especially poly(3-hexylthiophene) (P3HT) has been studied intensively. P3HT has favourable electronic and optical properties and a good processability. Furthermore, it has a strong tendency to crystallize.

Well-developed crystals of P3HT have a fibrillar shape, can be several micrometers long and have a cross section of approximately 20 × 4 nm.[1-3] More importantly, these fibres have been identified as the main hole conducting channels in optimally annealed, state-of-the-art bulk heterojunction solar cells (BHJSC) [4] and field-effect transistors (FETs).[5]

Crystallization already occurs upon solution deposition under fast drying conditions like with spin-coating. Crystallinity can be enhanced, in general, by slowing down the drying speed (low spin speeds, drop casting, dip-coating[5-7] whether or not in combination with high boiling solvents)[8, 9] and also by post-production treatments like 'thermal annealing'[10, 11] and exposure to solvent vapour ('solvent vapour annealing').[12] All these methods increase the time available for the molecules to order and hence promote fibre formation.

In most devices (BHJSCs and FETs) studied up till now, the fibres were formed during thermal annealing of the active layer. It has however long been recognized that these fibres can also be formed in solution.[1] Bottom gate, bottom gold (Au) contact FETs made from P3HT fibres deposited from *p*-xylene have demonstrated hole mobilities of up to 0.06 $cm^2 V^{-1} s^{-1}$ for single fibres.[13, 14] This value is not far from the best values that have been obtained for conventionally prepared P3HT FETs of comparable design (0.25 $cm^2 V^{-1} s^{-1}$).[15] Recently, it has been shown that 3.5% efficient P3HT-PCBM solar cells can be directly processed from nanofibre solutions without annealing.[3]

The direct deposition of nanofibre dispersions offers a highly attractive alternative to conventional processing from good solvents since it does not require a thermal treatment step. Therefore, it allows for the use of, for instance, flexible, transparent substrates like polyethylene terephthalate (PET). PET has a T_g of around 75 °C, which is incompatible with conventional heat treatment for P3HT, typically around 140 °C. Additionally, processing from nanofibre dispersions, or more general, nanoparticle dispersions, may offer a better control over the final morphology and crystallinity of the active layer as has been demonstrated for P3HT:PCBM solar cells.[3, 16] It may also allow for the processing of polymers with low solubilities, as has been demonstrated with poly(3-butylthiophene) fibre-based solar cells.[17, 18]

One of our research goals is to establish the effect of the alkyl side chain length of P3*A*Ts on device properties. It is a common believe[19] that P3HT offers the best compromise between electrical conductivity and solubility/processability where conductivity decreases and solubility increases with increasing side-chain length. This believe is based mainly on FET studies that compare the hole mobility of spin-coated layers of several P3*A*Ts casted from one solvent with, or without annealing. However, high temperature annealing, which for P3*A*Ts typically is performed well below the melting point (for P3HT at 140 °C *vs* mp at 220 °C) does not guarantee that fully relaxed systems are obtained. The nanofibre approach offers an attractive way to study the influence of alkyl chain length on material and device properties on a more equal footing, since nanofibre formation by crystallization in solution is expected to give more evolved and relaxed systems than those that can be obtained by thermal annealing. It also offers morphology control beyond what can be reached in conventional ways.

Although a few reports have addressed the formation of P3*A*T nanofibres from solution,[1, 17, 18, 20-22] more systematic studies are still scarce and it is not yet clear what solvents are most suitable for nanofibre formation. In this study we have addressed this issue for all P3*A*Ts with *n*-alkyl side chains that contain in between 3 and 9 carbon atoms ($3 \leq A \leq 9$). A selection of solvents and fibre formation conditions were found that give high yields of fibres (>60%) that have a high internal order, without (extensive) formation of larger aggregates, at concentrations suitable for device preparation (order of 0.1−1 wt. %). The isolated fibres were further characterized by AFM, UV-Vis spectroscopy and XRD.

2. Results

In order to avoid confusion and for consistency we will proceed with using the abbreviations P34T, P36T and P38T instead of commonly used P3BT, P3HT and P3OT for poly(3-butylthiophene), poly(3-hexylthiophene) and poly(3-octylthiophene).

2.1 Polymer synthesis and properties

The regioregular P3*A*Ts used in this study were synthesized by us from 2,5-dibromo-3-alkylthiophenes using the Rieke method (Experimental Part and SI_Figure 1). Salts and low molecular weight (MW) material were removed by Soxhlet extraction with methanol and hexane, respectively. This yielded polymers P33T to P39T in 50—80% yield with high regioregularities (*RR* ≥ 94.5%) (**Table 1**). Molecular weights were measured with GPC *versus* a polystyrene standard in chlorobenzene. The $\bar{M}_n$ values obtained for P34T to P39T are in a fairly narrow range; between 16.7 and 28.0 kg · mol^{-1}. It is well known for P36T that GPC overestimates $\bar{M}_n$ by a factor of ~2.0.[23-25] Hence the absolute $\bar{M}_n$ for our P36T is estimated at 11.9 kD which corresponds to a degree of polymerization DP_n of 71 and to a contour length l_n of 28 nm (using a value of 7.84 Å for the crystallographic *c*-axis[26]).

Table 1. Characterization data of the studied P3*A*Ts (see also **Table 2**).

		GPC[1)]		^{1}H-NMR	UV-Vis[2)]		DSC[7)]	
A	Yield[3)] (%)	$\bar{M}_n$ /10^3	*PD*	*RR*[4)]	λ_{max} / nm ($CHCl_3$)	λ_{max} /nm (TCB)[5]	T_m / °C (peak)	ΔH / J · g^{-1}
3	66	[6)]	[6)]	96.1	[6)]	467	285	30
4	75	19.5	2.29	96.5	[6)] [449]	468	281	28
5	79	16.7	1.93	94.5	451	469	249	29
6	80	23.7	1.80	94.5	450 [456]	471	234	24
7	67	24.4	1.64	97	451	471	198	20
8	73	28.0	1.66	97	451 [451]	469	210	20
9	50	25.9	1.46	98	449	467	187	23

[1)] GPC values reported versus polystyrene standards at 60 °C in chlorobenzene. [2)] Data in square brackets are from ref. [27]. [3)] Yield determined with respect to the amount of organozinc monomer. [4)] Regioregularity as determined by the ratio of the α-methylene protons that represent HT and non-HT couplings. [5)] Measurements performed at 26 °C in 1,2,4-trichlorobenzene (TCB). [6)] Low solubility impeded accurate measurements. [7)] Data of second heating run.

The solubility of P33T in chlorobenzene was too low for GPC analysis. The melting point and the absorption maximum at 467 nm (recorded in 1,2,4-trichlorobenzene) are, however, in agreement with the trends observed for the other polymers. Moreover, the width of the fibres obtained for P33T (~20 nm, *vide infra*) was identical to that of the other polymers. This, and the identical way of synthesis, all indicate that P33T has a *DP* comparable to that of the series P34T—P39T.

UV-Vis absorption spectra of the (well-dissolved) polymers obtained in $CHCl_3$ display a π-π* transition peaking around 450 nm.[28] The position of the maximum is quite insensitive to alkyl chain length.[27] Since our P33T and P34T could not be completely dissolved in $CHCl_3$, another solvent, 1,2,4-trichlorobenzene, was used to compare the solution spectra of the whole series. Only slight variation of λ_{max} with alkyl chain length was observed, reaching a maximum value of 471 nm for P36T and P37T and the lowest value of 467 for P33T and P39T (**Table 1**).

2.2 Fibre formation and isolation

Fibres were prepared by the slow cooling to room temperature (r.t.) of a heated, orange-coloured solution of P3*A*T in a suitable solvent.[1, 3] For each polymer several solvents were tested for suitability as fibre-forming solvent in the concentration range from 0.1 to 2 wt %. Some criteria and guidelines were used for solvent selection. Firstly, in view of device preparation, an appreciable amount of fibre (> 50 %) had to be formed *without* the formation of other, usually larger, precipitates as observed in UV-Vis. To allow for spin-coating layers of sufficient thickness (>20 nm), we aimed at fibre formation in the concentration range of ~0.3 to 1 wt %. Higher concentrations would cause gelation, resulting in nonuniform layers upon spin-coating, while lower concentrations would give layers of insufficient thickness. Secondly, solvents which are known as good solvents for fullerenes and solvents with a boiling point not deviating too much from that of *p*-xylene (138 °C), were favoured. *p*-Xylene is a suitable fibre forming solvent for P3HT.[1, 3, 13]

It turned out that there is not one solvent that even fits the first requirement for all polymers we used. For most solvents tested, the solubility of individual P3*A*T polymer chains increases with increasing alkyl side chain length. This is also the case for the dispersibility of the fibres. Therefore,

for a given solvent, high yields of dispersible fibres were only obtained for 1 to 3 polymers (with consecutive side chain lengths) in the concentration range of 0.3 to 1 wt %. The fibre yield was found to be rather insensitive to concentration in this range. The polymer-solvent combinations that were selected for fibre formation are listed in **Table 2**.

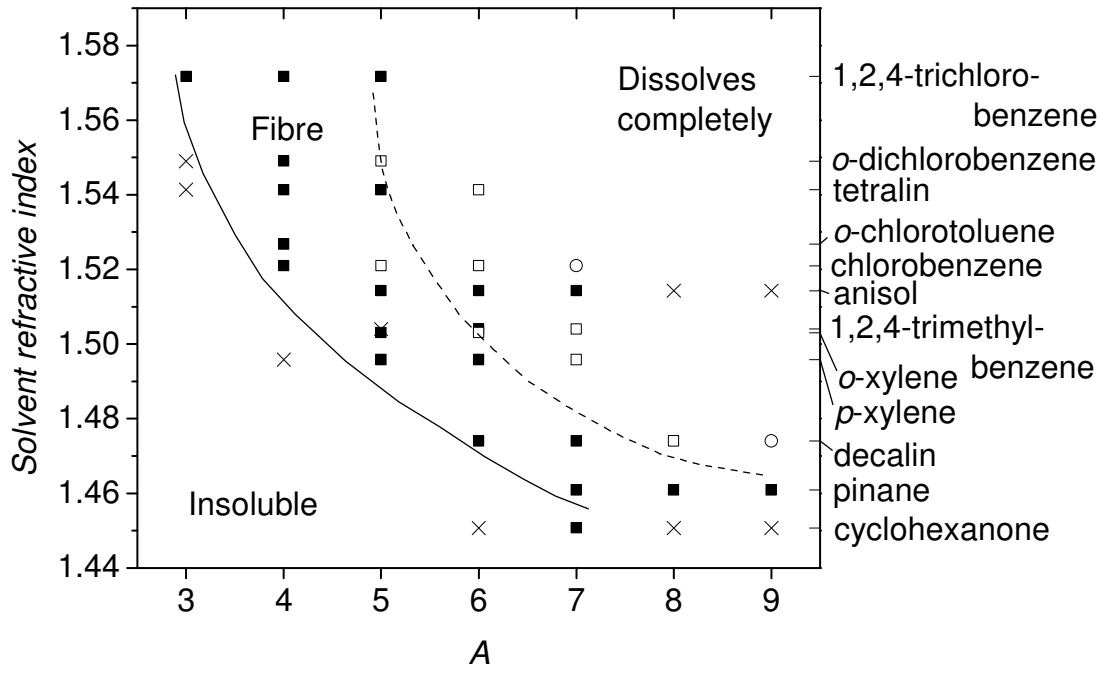

Figure 1 Fibre formation in function of solvent refractive index for 0.3 – 1 wt % polymer solutions as observed at room temperature. Indicated are: (×) polymer-solvent combinations that (in the 0.3 – 1% concentration range), besides fibres, also gave larger precipitates as observed in UV-Vis; polymer-solvent combinations that gave (■) over 50% fibre formation, and (□) less than 50% fibre formation; (○) combinations that afforded no fibre at all, or less than 5% fibre. Indicated are the approximate solubility limit at room temperature (solid line; 100% fibre formation) and the line of approximately 50% fibre formation (dashed line).

Previously, attempts have been made to relate the solubility of P3*A*Ts and the tendency to form nanofibres to the difference in solubility parameter δ between solvent and polymer.[22, 29] The single variable or Hildebrand solubility parameter concept offers a crude way to organize polymers and solvents in terms of cohesive energy density.[30, 31] A given polymer will likely dissolve in a given

solvent if their solubility parameters are similar. In this view, a certain but not too large difference in solubility parameters between polymer and solvent is needed for fibre formation.

Unfortunately, δ values are not known for all polymers and solvents used in this study and the values that are known do not seem to be able to predict fibre formation very well. We observed that for aliphatic hydrocarbon and (chlorinated) aromatic hydrocarbon solvents the solvent refractive index n_D has an equal or better predictive value in determining if the solvent will be a suitable solvent for fibre formation. In **Figure 1**, we plotted polymer-solvent combinations that gave fibre formation in the 0.3 – 1 wt % concentration range without forming larger precipitates as a function of n_D and alkyl chain length. Also indicated are lines for 100% and 50% fibre formation. From **Figure 1** it becomes clear that the n_D value of the solvent needed for fibre formation decreases with increasing alkyl chain length. For P34T and P35T the n_D range of solvents suitable for fibre formation is relatively large. It decreases for P3*A*Ts with longer alkyl side chains, while for P33T it is limited by the availability of solvents with high enough refractive indices (or dispersive type cohesive energy densities, see below).

It is known that n_D can be associated with the dispersive term δ_D in the Hansen solubility parameter concept *via* $\delta_D = 19.53 \cdot n_D - 11.35$ (for δ_D in $MPa^{1/2}$).[32, 33] In the Hansen solubility parameter model, the Hildebrand parameter δ is divided in three components due to dispersive (δ_D), polar (δ_P) and hydrogen bonding interactions (δ_H) as $\delta^2 = \delta_D^2 + \delta_P^2 + \delta_H^2$.

It should be noted that the lines of 50 and 100% fibre formation in **Figure 1** are concentration dependent. For example, while *p*-xylene was found to be a good solvent for fibre formation for P36T and P35T, it could also be used for P34T, but only at lower polymer concentrations (~0.1 wt %). Two solvents in **Figure 1** that behave unlike the other solvents are cyclohexanone and anisol. The latter solvent has been claimed to be more appropriate for fibre formation than for example *p*-xylene with respect to fibre yield.[22] We found that at concentrations between 0.1 and 1% it is suitable for the formation of fibres for P34T to P37T. Nevertheless, in our hands larger precipitates were obtained for P38T and P39T and pinane was to be preferred over anisol. Within the Hansen model, the anomalous behaviour of anisol and cyclohexanone can be attributed to the relatively high

hydrogen (δ_H) and also polar contributions (δ_P) of these solvents to δ.[34] These contributions may also explain the difference between anisol and cyclohexanone on one hand and chlorobenzene on the other, which all have similar Hildebrand parameters (19.5, 19.6, and 19.6 $MPa^{1/2}$, respectively).[30, 31]

For all polymers, the formation of fibres was accompanied by a change in the colour of the solution from clear orange to dark red or purple and by an increase in the viscosity. In UV-Vis absorption spectroscopy, the absorption band at 445—467 nm was replaced by a bathochromically shifted band with vibrational structure.

For P33T in 1,2,4-trichlorobenzene, fibre formation was complete within a few hours, even at concentrations as low as 10^{-4} wt %. For P3*A*Ts with alkyl chains between 4 and 7 carbon atoms, fibre formation was completed in 2 to 4 days while for P38T and P39T it took up to 10 days to complete fibre formation (as judged from UV-Vis spectrum). For the polymer-solvent combinations in **Table 2**, fibre formation was completed in less than 0.5 to 14 days and the time needed for fibre formation to go into completion increased with alkyl chain length. It was also noted in many cases that freshly formed fibres dissolve at lower temperatures upon reheating than fibres that have aged for 1 to 2 days. Apparently, after formation, some reorganization still takes place. In one case, P35T in 1,2,4-trimethylbenzene, the fibres could not completely be redissolved upon heating after formation.

Table 2 Solution UV-Vis absorption maxima λ_{max} and molar attenuation coefficients[1)] ε_T of polymers P3*A*T, well-dissolved in solvents for fibre formation, at 20 °C, together with UV-Vis, GPC[2)] and fibre yield data on fibre and well-dissolved polymer fractions obtained after centrifugation of pristine fibre dispersions.

	solvent[3]			pristine polymer			fibre					non-fibre	
A	name	Bp / °C	n_D	λ_{max} /nm	ε_T /10^3 /M^{-1} cm^{-1}	*C* (wt %)	yield[4] (%)	λ_{max}[5] /nm	$A_{0\text{-}0}/A_{0\text{-}1}$[8]	M_n /10^3	*PD*	M_n /10^3	*PD*
3	1,2,4-trichlorobenzene	214	1.5717	467	8.27 ± 0.23[6]	0.3	[7] / 98.5	**475** (467), 512, 555, 611	0.43	[7]	[7]	[7]	[7]
4	tetralin	208	1.5413	452	7.85 ± 0.03	0.5	90 / 84	460, 490, **516** (521), 563, 616	0.52	23.2	2.11	6.52	1.64
4	*o*-chlorotoluene	159	1.5268	456	7.83 ± 0.03	1	95 / 94	460, 490, **517** (521), 562, 616	0.51	22.6	2.06	7.16	1.66
5	*p*-xylene	138	1.4958	454	8.17 ± 0.04	0.5	75 / 76	453, 485, **522** (519), **556** (559), **605** (607)	0.78	24.8	1.56	8.23	1.51
6	*p*-xylene	i.d.	i.d.	455	8.48 ± 0.02	1	76 / 77	455, 487, **524** (521), **559** (562), **607** (609)	0.86	29.7	1.61	13.8	1.62
7	*cis*/*trans*-decalin	190	1.474	447	8.53 ± 0.03	1	91 / 86	267, 503 , **545** (547), 592	0.95	24.8	1.67	10.7	1.44
7	pinane	165	1.4609	446	8.08 ± 0.03	0.5	100 / 98.5	503 , **541** (544), **580** (589)	0.95	23.0	1.69	7.82	1.40
8	pinane	i.d.	i.d.	446	8.53 ± 0.03	0.5	94 / 92	273, 454, 488 , **527** (522), **561** (563), **609** (612)	0.88	31.1	1.56	13.6	1.30
9	pinane	i.d.	i.d.	445	8.51 ± 0.03	0.5	87 / 82	455, 488 , **527** (522), **562** (564), **609** (613)	0.87	26.9	1.51	14.9	1.36

[1] ε_T = molar attenuation coefficient based on `molar monomer concentration´. [2] Conditions: chlorobenzene; 60 °C; MW reported *versus* polystyrene standards. [3] Boiling points and refractive indices from ref [35]. or, in case of *cis*/*trans*-decalin, the supplier. [4] Fibre yield based on fitting the GPC trace (left) and the UV-Vis spectrum (right) (see text). [5] Bold numbers are real maxima, normal numbers were obtained *via* fourth derivative analysis. [6] P33T has a very strong tendency to form fibres, even at concentrations as low as 10^{-4} wt. %. The low concentrations that had to be used consequently introduce a larger error. [7] Low solubility impeded the measurement. [8] The reduced absorption spectrum, *i.e.* A/ν *versus* ν was used to determine $A_{0\text{-}0}/A_{0\text{-}1}$.

Pure fibres were obtained by centrifugation of the pristine fibre dispersions (see Experimental Part). The isolated fibres were then centrifuged 5 times with clean solvent to remove any well-dissolved polymer. For every polymer, the isolated fibres and the supernatant of the first centrifugation (that contained most of the well-dissolved polymer) were characterized with GPC (**Table 2**, and **SI_Figure 3** in Supporting Information). Fibre formation was found to be accompanied by molecular weight fractionation. The M_n values of (re-dissolved) polymer from fibres had increased to 102–148% of their overall values, while those for non-aggregated polymer in solution had reduced to 33–58%. Due to this fractionation, also the polydispersity of the polymer fraction incorporated in the fibres reduced significantly for many of the polymers. This effect was more pronounced for polymer-solvent combinations that had relatively low fibre yields (see below; P35T and P36T) and for polymers with a relatively low M_n (P35T).

The MW fractionation upon fibre formation indicates that high MW polymer chains tend to precipitate first. Increasingly lower MW material then is incorporated in the fibres until a certain lower MW boundary has been reached. It can be expected that besides a high MW also a high *RR* of the individual polymer chain increases its tendency to precipitate.

The mechanism of fibre formation has been investigated in detail for P36T and P3(12)T in xylene.[36] It was concluded that fibre formation is a two-step process. In the first step, the polymer chains undergo a coil-to-rod conformational change, while in the second step the rod-like polymer chains crystallize to form a fibre. It was found that an increase in alkyl chain length reduces the overall energy barrier for fibre formation. However, while for P36T the crystallization step had the highest activation energy and appeared to be the rate-limiting step, for P3(12)T this was the rod-to-coil transformation.

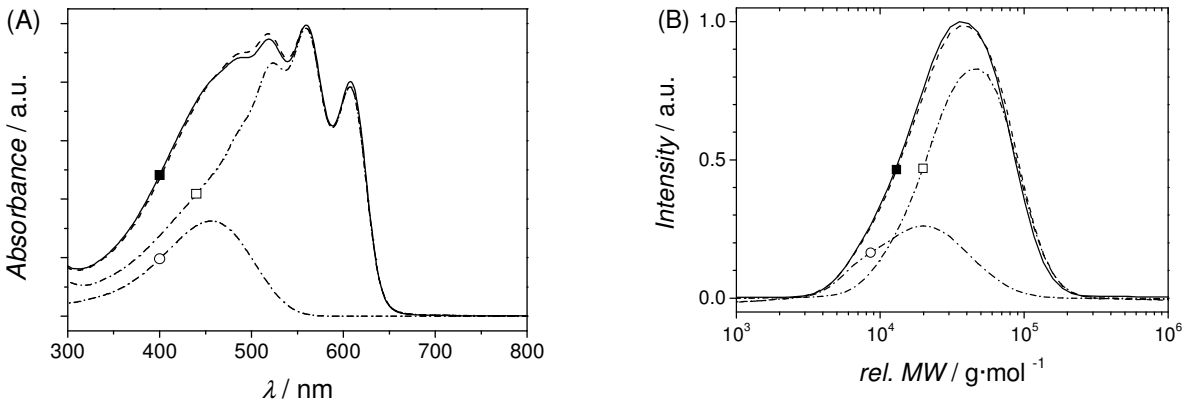

Figure 2 (A) UV-Vis absorption spectrum of a pristine P36T fibre solution in *p*-xylene (■, solid line) together with the fitted spectrum (■, dashed line) as a sum of the pure fibre (□) and `amorphous´ (○) spectra. (B) GPC curve of pristine P36T polymer (■, solid line) together with the fitted curve (■, dashed line) as a sum of the GPC of the pure fibre (□) and well-dissolved part (○).

The MW fractionation enabled the fibre yield to be determined on the basis of the obtained GPC traces (see **Figure 2**B and **SI_Figure 3**). By fitting the GPC trace of the pristine polymer as a sum of the GPC traces of the pure fibre and well-dissolved polymer fractions, the yield of fibre formation could be calculated for P34T to P39T as the area under the fibre trace divided by the area under the pristine polymer trace (in a Δn_D *versus* 'log MW' representation).[37] The fibre yields obtained in this way are in the 75—95 % range for the polymer-solvent combinations presented here.

The fibre yield was also determined with UV-Vis spectroscopy (see **Figure 2**A and **SI_Figure 2**). To this end, the absorption spectrum of the pristine gel was fitted as a sum of the pure fibre absorption spectrum (obtained after fibre isolation) and the corresponding absorption spectrum of well-dissolved polymer. Yields determined with this method (**Table 2**) are in excellent agreement with those obtained with GPC. For P39T it was found that the fibre yield was very sensitive to temperature around room temperature. Slight heating quickly dissolves fibres into individual polymer chains and reduces the fibre content.

2.3 Fibre characterization

The fibres isolated by centrifugation were characterized with AFM, TEM, XRD and UV-Vis spectroscopy.

2.3.1 Morphological study (AFM and TEM)

Tapping mode AFM height and phase images of fibres of P33T to P39T from several solvents are given in **Figure 3**. The fibres were deposited on an SiO_x covered monocrystalline silicon (100) surface by dipping the silicon substrate in a diluted (0.05 wt %, unless indicated otherwise) pristine fibre solution for 1 minute followed by blowing off excess solvent with an N_2 stream. For TEM and XRD, dispersions of fibres isolated by centrifugation were spin-coated or drop-casted and examined. Bright-field TEM images and SAED (selected area electron diffraction) patterns of fibres in selected solvents are also given in **Figure 3**.

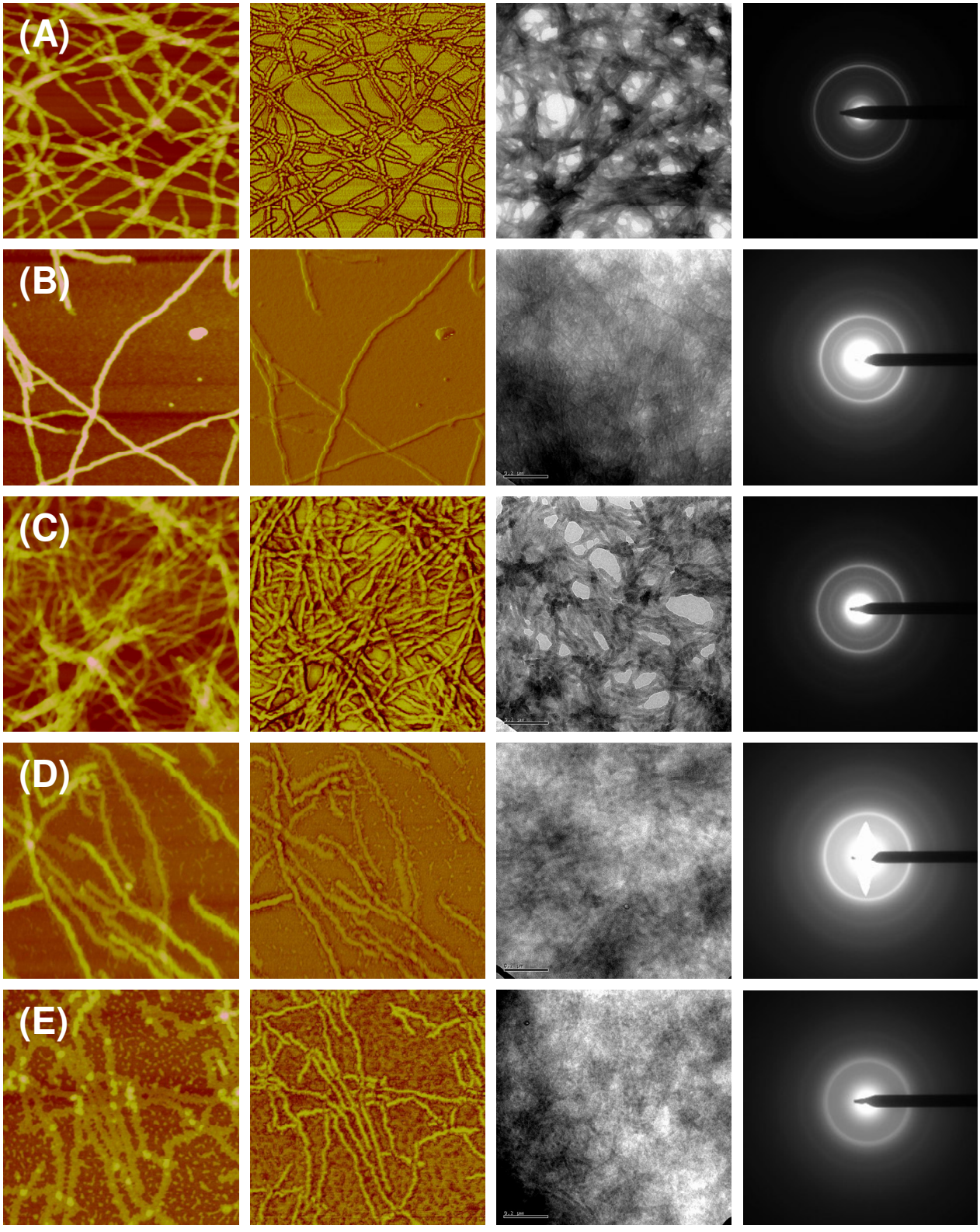
(A)
(B)
(C)
(D)
(E)

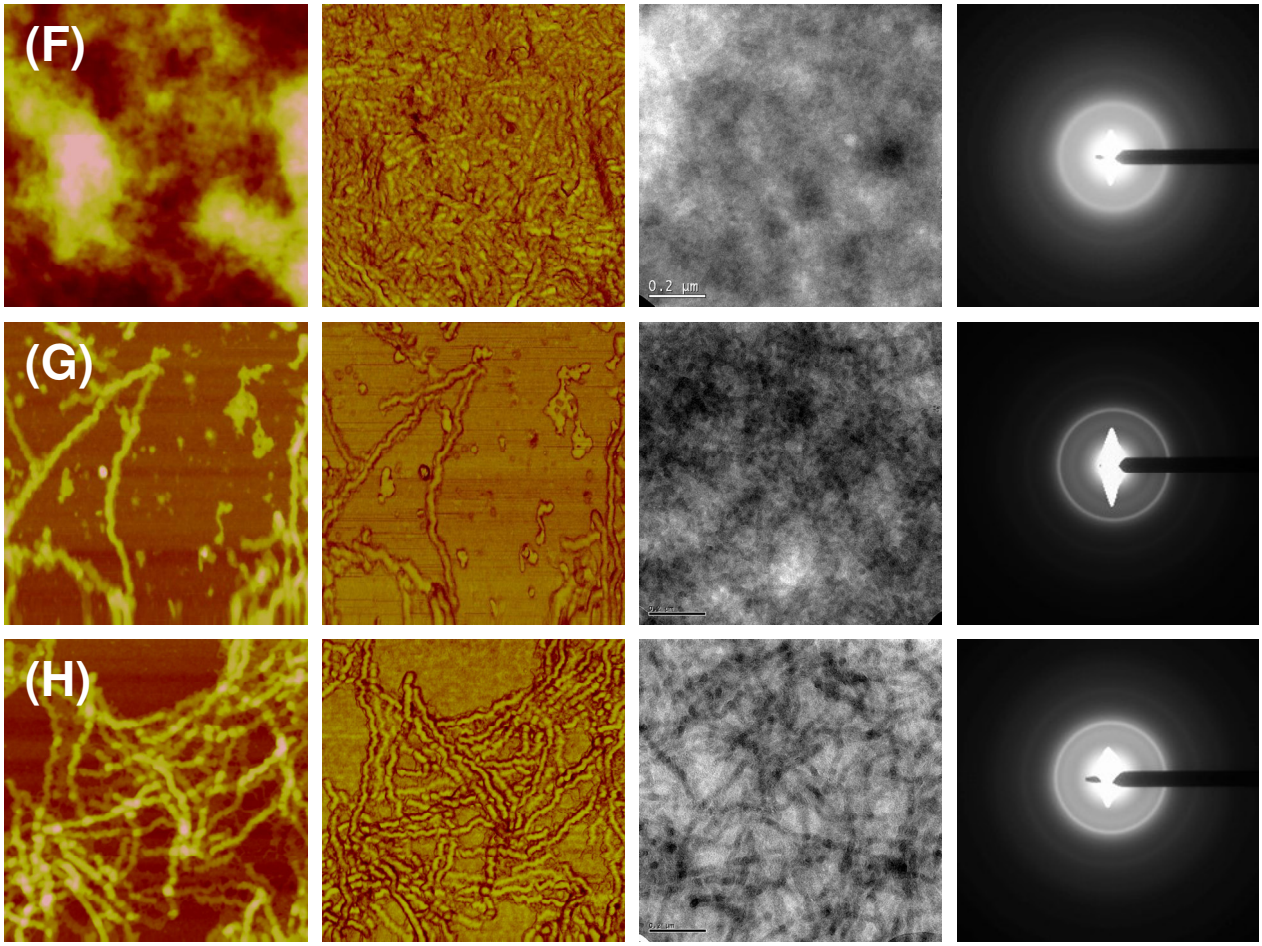

Figure 3 From left to right: tapping mode AFM height and phase images (1 × 1 μm) of P3*A*T fibres on SiO_x/Si (100), and bright-field TEM (1.06 × 1.06 μm) images of isolated fibres spin-coated on glass together with the SAED patterns for (A) P33T in 1,2,4-trichlorobenzene, (B) P34T in tetralin, (C) P35T in *p*-xylene, (D) P36T in *p*-xylene, (E) P37T in *cis*/*trans*-decalin, (F) P37T in pinane, (G) P38T in pinane, (H) P39T in pinane.

For all polymer—solvent combinations used, the fibres are 20 +/- 5 nm wide and 0.5 to >4 μm long. Thicknesses were found to vary between 2 and 10 nm (**Table 3**). A clear increase in the thickness of the fibres with alkyl chain length was not observed. Using SAXD, Ihn *et al.* [1] have found that the P36T fibres they obtained from solution had a thickness of 2 to 5 nm (2 to 3 polymer chains). For P36T down to P33T, AFM shows that the fibres have an increasing tendency to form bundles of fibres.

Table 3 AFM data on fibres of P3*A*T deposited on SiO_x/Si (100). X-Ray diffraction data (2θ values and unit cell parameter *a*) on the 100 reflection of drop-cast P3*A*T isolated fibre films on SiO_x/Si (100). The Scherrer length ξ is based on the width of a Split-Pearson VII peak fitted to the (100) diffraction peak.

		AFM	TEM	XRD		
A	solvent	thickness / nm	*b* / Å	2θ / °	*a* / Å	ξ / nm
3	1,2,4-trichlorobenzene	5-10	3.0, 3.5, 3.7, 4.8, 10.6	8.37	10.55	9.5
4	tetralin	5	3.8, 5.3	7.22	12.24	9.5
4	*o*-chlorotoluene		3.8, 5.2	7.29	12.11	10.1
5	*p*-xylene	5	3.7, 5.0	5.95	14.83	13.2
6	*p*-xylene		3.8, 5.1	5.59	15.79	12.0
7	*cis*/*trans*-decalin	2	3.9	5.08	17.38	8.4
7	pinane	3	4.0	5.15	17.14	8.6
7	pinane, 10 min @ 70 °C		3.8	4.84	18.25	14.8
8	pinane		3.8, 4.5[1)]	4.53	19.47	13.5
9	pinane	5-10	3.8, 4.4[1)]	4.15	21.27	14.5

[1)] Very diffuse diffraction ring.

2.3.2 Structural model of isolated P3*A*T fibres

X-ray diffraction (XRD) (**Figure 4**) on drop-casted layers and selected area electron diffraction (SAED) (**Figure 5**) on spin-coated layers were used to characterize the crystalline structure of the isolated P3*A*T fibres. XRD spectra were recorded in a coupled θ-2θ-geometry, which ensures that only crystal planes parallel to the substrate surface are probed. The diffraction data are given in **Table 3**. All fibres gave 'crystalline' diffraction patterns. The amorphous halo typically observed around 20° for solution casted layers of P3*A*Ts[26] is very weak, indicating that the fibres are all highly crystalline.

(A) (B)

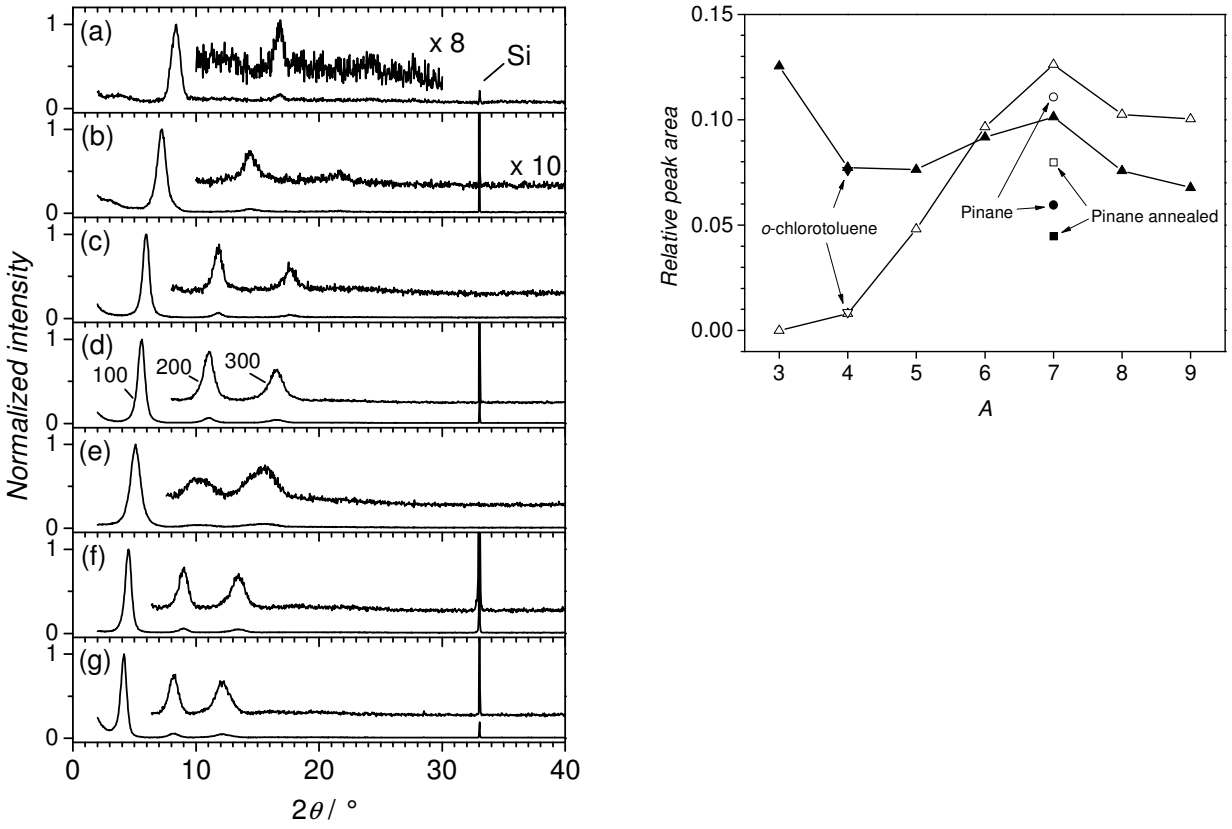

Figure 4 (A). XRD diffraction patterns of drop-casted films of isolated P3*A*T fibres obtained from the solvents listed in **Table 2** on SiO_x/Si(100) for (a) P33T, (b) P34T from tetralin, (c) P35T, (d) P36T, (e) P37T from *cis*/*trans*-decalin, (f) P38T, (g) P39T. Intensity enlargement of the insets is ×8 for P33T and ×10 for P34T–P39T; (B) Peak areas of the (200) (filled symbols) and (300) (open symbols) reflection relative to the (100) reflection as a function of the number of carbon atoms *A* in the side chain. Additional points have been added for P34T fibres from *o*-chlorotoluene (▼) and P37T fibres from pinane (both non-annealed [●/○] and annealed [■/□] for 10 min at 70 °C).

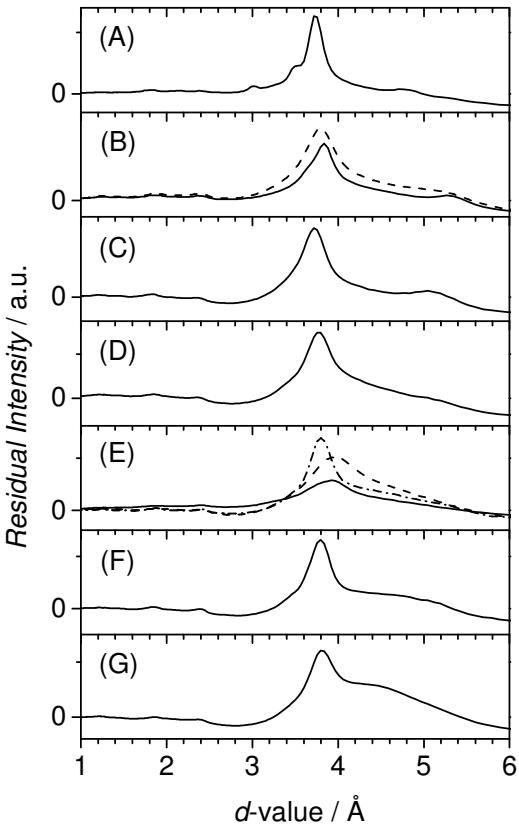

Figure 5 SAED residual intensity patterns of isolated P3*A*T fibres spin-coated on glass for: (A) P33T in 1,2,4-trichlorobenzene; (B) P34T in tetralin (solid line) and *o*-chlorotoluene (dashed line); (C) P35T in *p*-xylene; (D) P36T in *p*-xylene; (E) P37T in *cis*/*trans*-decalin (solid line), pinane before (dashed line) and after annealing for 10 min at 70 °C (dash-dot line); (F) P38T in pinane; (G) P39T in pinane.

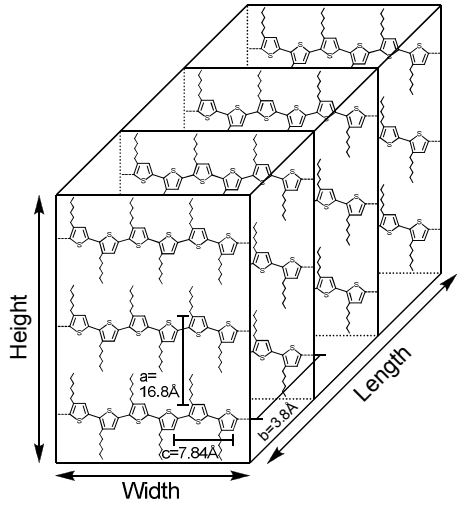

Figure 6 Schematic of a fibre (Reprinted with permission from ref. [14]. Copyright 2004 American Chemical Society.)

For P3*A*Ts crystallized from solution, at least two crystal structures are known, usually indicated by the numbers I and II.[1, 26, 38, 39] The type I crystal structure is most commonly observed. In the very basis, it can be described by an orthorhombic unit cell, while more advanced studies suggest a monoclinic unit cell with the monoclinic angle close to 90° (**Figure 6**). In this form, the polymer chains are oriented along the *c*-axis, perpendicular to the fibre axis or *b*-axis. The alkyl side chains point mainly in the direction of the *a*-axis, which scales linearly with alkyl side chain length. The polymer chains stack their planarized π-systems in the *b*-direction and these stacks pile up in the *a*-direction, forming layers of a lamellar structure which make up the height of the fibre. The typical π-stacking distance in the type I structure is 3.8 Å and the alkyl side chains do not interdigitate. Instead, they are tilted away from the thiophene backbone plane by *ca.* 30° as to efficiently fill up the space between them.

The type II crystal structure resembles the structure of type I, but is believed to have the alkyl side chains interdigitated.[39] This results in a *ca.* 30 % shorter *a*-axis that has a smaller dependence on the alkyl side chain length then for type I.[39, 40] To allow for side chain interdigitation, the π-stacking distance (taken to equal the lattice constant *b*) is increased from 3.8 to 4.7 Å for P38T.[39]

With the exception of P37T (see next section), the observed reflections in XRD for all fibres can be assigned to the (100), (200) and (300) reflections within the orthorhombic framework of the type I form. The intensity of the higher (300) reflection relative to that of the (100) reflection was found to increase with increasing alkyl length up to $A = 6$ (**Figure 4**) while that of the (200) reflection remained almost indifferent with alkyl chain length. This trend can be attributed to an increasing order in the direction of the *a*-axis with increasing alkyl chain length in going from P33T to P36T. Similar observations have been made for films of a series of four *ca.* 80 % regioregular P3*A*Ts with *A* values of 0, 4, 6, and 12 by Tashiro *et al.*,[41] who observed a 'lowering of the rate of intensity decrement in the series of (*h*00) reflections with increasing alkyl chain length', coupled with a narrowing of the half width of the (*h*00) reflections with increasing alkyl chain length.

The Full Width at Half Maximum (FWHM) of the XRD diffraction peaks can be related to a crystal size by using the Scherrer equation: FWHM $(2\theta) = 0.9\ \lambda / \xi \cdot \cos\ \theta$, where ξ equals the

crystallite size, λ the wavelength of the radiation and θ the angle of incidence. For P33T and P34T, ξ is around 10 nm. Higher values, between 12 and 15 nm, were obtained for P35T to P39T (excluding P37T).

The SAED data support the assignment to the type I form with the diffraction peaks at *ca.* 3.8 Å, presumably mainly due to the (010) reflection of form I with a minor contribution of the (002) reflection.[1, 26] For P33T to P36T also a weak but distinct diffraction ring around 5 Å is visible. This is likely to be due to the presence of a small amount of the interdigitating phase II. For P38T and P39T a broad peak around 4.5 Å is visible, which could also be due to the presence of some phase II. No evidence was found in XRD, however, for the presence of type II and other phases.

For P33T even more diffraction peaks are discernible in the SAED pattern. Remarkably, the (100) reflection is also visible (10.6 Å) as a ring with a very small radius. The (100) reflection was not observed in the SAED patterns of the other P3*A*Ts. Although the presence of additional phases cannot be excluded, we therefore attribute the additional peaks and the (100) reflection in SAED to a less pronounced preferential orientation of the P33T fibres relative to the substrate. This is most likely caused by the bundling of the fibres as was observed with AFM (*vide supra*); the fibres in these bundles apparently lack the freedom of movement to orient to the substrate independently of the other fibres.

The (010) reflection would be expected in XRD around 23.4° (3.8 Å), see **Figure 4**A, but there it is totally absent, indicating that, in contrast to what is normally observed for spin-coated films from a good solvent, the drop-casted fibre layers are all highly oriented with the π-π stacking or *b*-direction in the plane of the film. The strong intensity of the (100) reflection in XRD for all fibres except those of P33T furthermore indicates that the *a* axis of these fibres is strongly oriented perpendicular to the substrate plane.

A linear regression of the *a* values *versus* the number of carbon atoms *A* in the side chain gives the following relation (see supporting information): a / Å = 5.12 + 1.79 · A. Previously, a slope of 1.8 has been found for P3*A*Ts cast from solution[42] and recently, a slope of 1.9 Å and intersection of 5.1 Å have been found for fibres obtained from anisol.[22] This indicates that the structure of the fibres

under consideration is identical to the type I phase previously found in the solid state for P3*A*Ts with even *A* values of 4 to 14 and also identical to the fibres from anisol (even *A* values of 4 to 10).

2.3.3 Structural model of isolated P37T fibres

For P37T fibres grown from *cis*/*trans*-decalin and pinane anomalous results were obtained in XRD, SAED and UV-Vis (*vide infra*). These results point to a structure that is slightly different from the normal orthorhombic type I structure. From UV-Vis it was deduced that the fibres from pinane consist of the most pure form of this new structure, while those from decalin contain a significant amount of the normal type I structure. We will therefore focus on the P37T fibres obtained from pinane.

The broadened (100) diffraction peak obtained for P37T fibres from decaline [pinane] gave rise to a relatively small crystal sizes ξ of 8.4 nm [8.6 nm]. The lattice constant *a* of 17.38 Å [17.14 Å] was found to be only marginally smaller than the 17.65 Å expected from interpolation. With SAED a broader halo was obtained for the (010) reflection than normally obtained for the type I structure, and the associated lattice constant *b* had increased from 3.8 to 3.9 Å [4.0 Å] (see **Figure 3** and **Figure 5**). The contraction of the *a* and expansion of the *b* lattice constants resembles the formation of a type II crystal structure. Nevertheless, even for the fibres from pinane the deviation of the lattice constants *a* and *b* is only 8 and 22% respectively of the change needed to convert type I into type II. Hence, the crystal structure obtained for P37T is interpreted to be a slightly modified type I structure that we will refer to as type I'.

2.3.4 UV-Vis spectroscopy and intermolecular coupling

The UV-Vis spectra of thin films of the isolated fibres of P33T to P39T are depicted in **Figure 7**. Absorption maxima are compiled in **Table 4**. It can be clearly seen that the increase in alkyl chain length in going from P33T to P35T induces a strong increase in the vibrational structure. Also the band maximum red-shifts with increasing alkyl side-chain length from 482 nm for P33T to 556 nm for P35T. For P35T to P39T with the exception of P37T, the band maximum undergoes a modest

red-shift from 556 nm to 562 nm. Simultaneously, the relative intensity of the first vibronic transition around 610 nm slightly increases at the cost of the third vibronic transition around 520 nm.

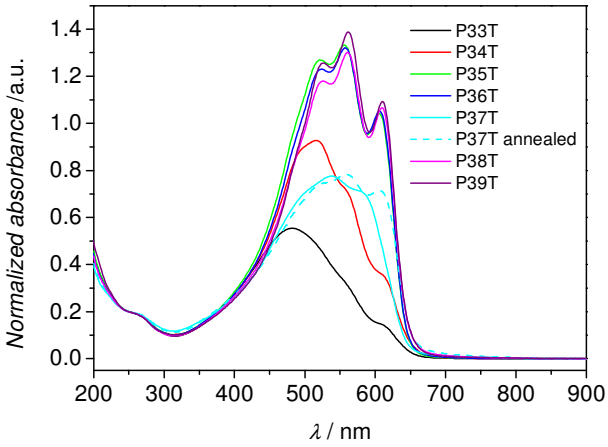

Figure 7 UV-Vis spectra (normalized for an absorbance of 0.2 at 250 nm) of drop-casted films of the isolated fibres of P33T to P39T (P34T from tetralin; P37T from pinane) on quartz.

Table 4 Solid state UV-Vis maxima in the range 250–900 nm and $A_{0\text{-}0}/A_{0\text{-}1}$ values for drop-casted films of isolated P3*A*T fibres obtained from the indicated solvents.

A	Solvent	λ_{max} /nm major component [1)]	$A_{0\text{-}0}/A_{0\text{-}1}$ [2)]
3	1,2,4-trichlorobenzene	272, **482**, ~521, 560, 614	0.49
4	tetralin	457, 487, **516** (523), 564, 618	0.55
4	*o*-chlorotoluene	277, 453, 488, **508** (523), 566, 620	0.52
5	*p*-xylene	273, 481, **521** (518), **556** (562), **606** (610)	0.85
6	*p*-xylene	272, 451, 482, **523** (518), **557** (563), **606** (613)	0.86
7	pinane	267, ~495, **537** (547), 593	0.98
7	pinane, annealed[4)]	272, 479, 517, **560** (567), **607** (622)	0.99
8	pinane	274, 453, 484, **526** (520), **560** (564), **610** (615)	0.89
9	pinane	274, 454, 487, **526** (521), **562** (565), **610** (615)	0.86

[1)] Bold numbers are real maxima, normal numbers were obtained *via* fourth derivative analysis. [2)] The reduced absorption spectrum, *i.e.* A/ν *versus* ν was used to determine $A_{0\text{-}0}/A_{0\text{-}1}$. [3)] Not observed. [4)] Annealed for 10 min at 70 °C.

The spectrum of P37T displays much less vibrational structure than observed for P36T and P38T. Fourth derivative spectroscopy reveals vibrational peaks at ~495, 547 and 592 nm for P37T fibres in the thin film as well as a peak at 621 nm which indicates that the normal type I form is also present. The first vibrational peak at 592 thus is blue-shifted by 0.075 eV as compared to the peaks observed for P36T (613 nm) and P38T (615 nm).

Recently, it has been shown theoretically[43, 44] and experimentally[45] that the absorption and emission of the lamellar organised aggregates of P36T can be described and understood in terms of an H-aggregate type chromophore with weak interchain coupling. The reduced intensity of the first (0-0) peak of the vibronic progression in absorption and emission as compared to those observed for isolated polymer chains (in solution) can be explained within this model.

In the H-aggregate, the 0-0 emission is symmetry forbidden, but weakly allowed by (spatially correlated) disorder of the transition frequencies of the individual polymer chains. The intensity of the 0-0 transition in absorption is reduced by increased exciton coupling. The magnitude of the interchain coupling energy W can be extracted from the intensity ratio of the first and second vibronic transitions ($A_{0\text{-}0}/A_{0\text{-}1}$) in the thin film absorption spectrum (when represented as reduced intensity *versus* energy). If the Huang-Rhys factor S is taken to be 1, which is the case for P36T[45], then: [43, 45]

$$\frac{A_{0-0}}{A_{0-1}} \approx \frac{n_{0-1}}{n_{0-0}} \left(\frac{1 - 0.24W / E_p}{1 + 0.073W / E_p} \right)^2, \qquad (1)$$

where $n_{0\text{-}i}$ is the real part of the refractive index at the 0-i peak and E_p is the energy of the vibration coupled to the electronic transition (0.18 eV for P36T). If it is assumed that the refractive index ratio $n_{0\text{-}1}/n_{0\text{-}0}$ is equal to 1 (for a P36T thin film a value of 0.97 has been measured)[45] and if the value for E_p of 0.18 eV is assumed to be valid for all polymers, W can be calculated on the basis of the $A_{0\text{-}0}/A_{0\text{-}1}$ obtained for fibre films (**Table 4**) and for fibres in solution (**Table 2**). **Figure 8** shows that W, independent of refractive index of the medium (thin film or fibre dispersion) decreases strongly in going from P33T (0.19 eV) *via* P34T (0.16 eV) to P35T for which it reaches a stable value of around 0.04 +/- 0.01 eV (except for P37T, *vide infra*). A lower value of W is associated with a larger

conjugation length and hence it can be seen that the conjugation length saturates with increasing side chain length at 5 carbon atoms.

For P37T fibres from pinane, a significantly lower value of $W \approx 0.01$ eV was obtained. From SAED (*vide supra*) we deduced a stacking distance for P37T of 4.0 Å that is significantly larger then for the other P3*A*Ts investigated. An increase in the interchain distance is expected to lead to a reduced interchain coupling and hence a reduced value of *W*. We therefore attribute the reduced value of *W* to an increased interchain distance for P37T, although an effect of the conjugation length cannot be excluded completely.

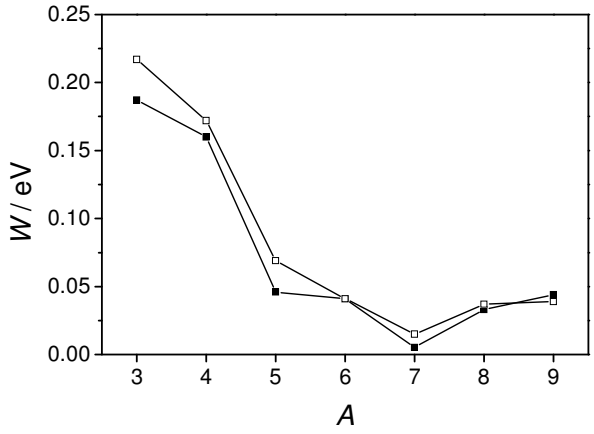

Figure 8 Free exciton bandwidth *W* as estimated for isolated P3*A*T fibres as a function of alkyl chain length in drop-cast films (■) and in solution (□). P34T fibres from tetralin and P37T fibres from pinane are shown.

2.3.5 Conversion of P37T from type I' to type I

Upon annealing a film of P37T fibres from pinane for 10 min at 70 °C, the XRD and SAED patterns of type I crystal are obtained (**Figure 9**, **Table 3**). In UV-Vis (**Figure 9**, **Table 4**), a red-shift is observed and the vibrational progression typical for type I is regained, albeit less pronounced than for P3*A*T fibres obtained directly in the type I form. Remarkably, the low free exciton bandwidth *W* retains its value of ~5 meV upon annealing, while the π-π stacking distance is reduced from 4.0 to 3.8 Å (**Table 3**). This suggests that the conjugation length is indeed much larger in P37T

fibres than in the other fibres.

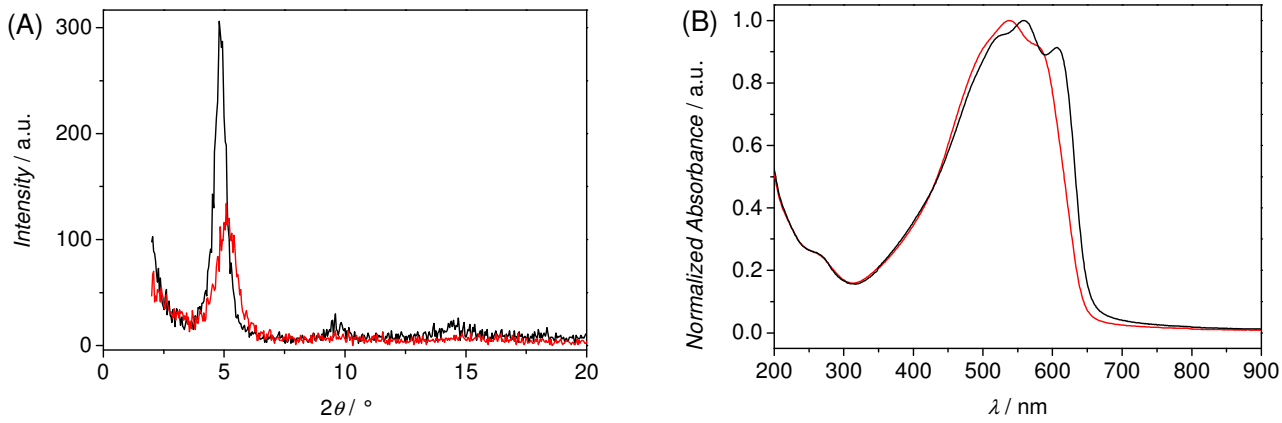

Figure 9 (A) XRD patterns and (B) solid state UV-Vis spectra of isolated P37T fibres from pinane before (red line) and after (black line) annealing for 10 min at 70 °C. Intensities cannot be compared.

The conversion to the type I crystal form was also attempted in solution. A 0.5 wt % dispersion of P37T fibres in pinane was kept at 50 °C and 60 °C and the evolution of the UV-Vis spectrum was followed in time (**Figure 10**, and **SI_Figure 5**). After 4 days, the solution was allowed to cool to room temperature and 24h later the last spectrum was recorded. At both temperatures the peaks at 541 and 580 nm associated with the type I' phase were slowly replaced by peaks at 522, 557 and 605 nm, characteristic for the type I crystal structure. Remarkably, upon cooling after 4 days, the polymer that crystallises from solution again crystallises in the type I' phase and not in the type I phase, preventing the formation of pure type I fibres in solution. This can be deduced from the disappearance of the vibrational structure in an identical way as is observed upon initial heating.

It is also remarkable that the UV-Vis spectrum obtained 1 day after cooling from 60 °C is virtually identical to thin film spectrum obtained upon spin-coating P37T from chlorobenzene solution (**Figure 10**B). This suggests that the phase I' obtained for P37T fibres could serve as a model for the kind of disorder encountered in P3*A*T films spin-coated from good solvents like chlorobenzene.

It is not well understood why only P37T has such a high tendency to form fibres of the type I' phase. It is known that the formation of the type II phase, which bears some similarities with the type I' phase, is favoured for low MW and lower (~80 %) *RR* P3AT samples.[40] Our P37T, however, does

not have a significantly lower MW or *RR* as compared to the other P3*A*Ts. The only sign of a possibly higher than average chain defect level is the slightly lower than expected m.p. as observed with DSC (**Table 1**). The interplay between solvent and polymer during fibre formation and more in particular the incorporation of solvent molecules in the fibres during their formation[46] could also play a role in the preferred formation of the type I' crystal phase.

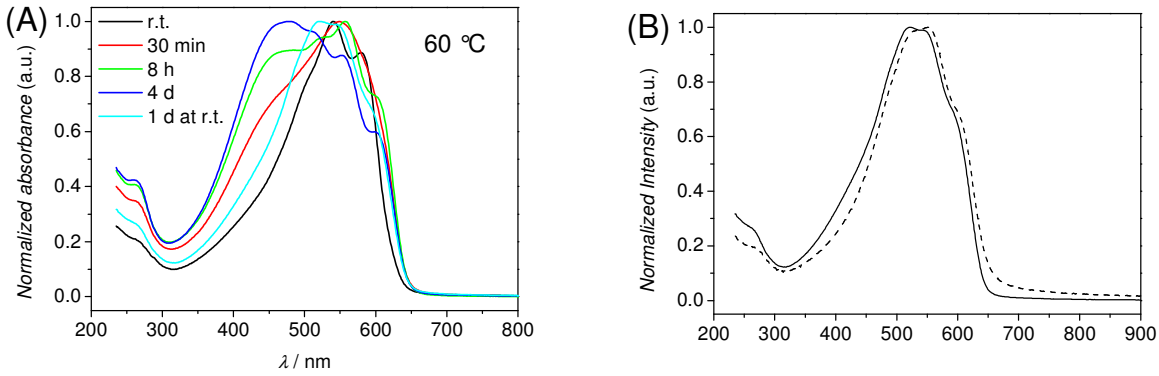

Figure 10 Time evolution of the UV-Vis spectrum of 0.5 wt. % P37T fibres in pinane at 60 °C (A) [for spectra at 50 °C; see Supporting Information]. Shown spectra were taken at room temperature, after 30 min, 8 h and after 4 days, when the solution was cooled to r.t. The last spectrum was taken 24 h after cooling to r.t. In B the spectrum obtained after 4 days at 60 °C and cooling to r.t. (solid line) is compared to the spectrum of a P37T film spin-coated at 2000 rpm from a 1 wt % solution chlorobenzene.

3. Conclusions

Efficient fibre formation for all regioregular poly(3-alkylthiophene)s with alkyl chain lengths between 3 and 9 carbon atoms has been accomplished in several solvents and fibres from selected solvents have been isolated by centrifugation and characterized. The fibre yield could be determined by both UV-Vis and GPC. It was observed that for the aliphatic and (chlorinated) aromatic hydrocarbon solvents used, the solvent refractive index offers a way to predict if fibre formation will be feasible or not (provided that the boiling point of the solvent is not too low).

Structural characterization of the fibres with AFM and TEM revealed that they are 2-5 nm in height, 15-25 nm wide and 0.5 to >4 μm long. All fibres, except for those of P37T, crystallized in the well-known type I non-interdigitating crystal form with a π-π-stacking distance of ~3.8 Å Evidence was obtained from SAED for the presence of small amounts of type II phase in almost all fibres. All fibres, except for P33T, were found to strongly orient with the *a* axis perpendicular to the substrate plane. The *a* axis of the P33T fibres was found to be less oriented with respect to the substrate plane. This was attributed to bundling of these fibres.

The order within the fibres was probed with XRD, SAED, and UV-Vis and was found to strongly improve with increasing alkyl chain length in going from P33T to P35T, resulting in a longer conjugation length. For P35T to P39T the improvement in order is only marginal.

Fibres from P37T, were found to mainly crystallize in a type I-like crystal that we refer to as type I'. This new crystal structure has a lattice constant *a* that is marginally shorter than that of phase I and a slightly longer lattice constant *b* of 4.0 Å and thus in XRD can hardly be distinguished from phase I. It is furthermore characterized by a blue-shifted absorption band in UV-Vis spectroscopy. The type I' fibres were converted into normal type I fibres in the solid state at 70 °C and in solution around 50 °C. In the solid state, this led to type I crystals with an increased conjugation length.

Future work will concentrate on the use of these nanofibres in both FET-devices and solar cells. It is believed that the use of nanofibres in these devices will allow us to better correlate materials properties with (opto-)electrical device characteristics.

4. Experimental

Solvents were used as received: *o*-xylene, *p*-xylene (both ≥99%) and pinane (>98%; isomer mixture) were obtained from Merck, decahydronaphthalene (≥98.0%; *cis*/*trans* mixture) and 1,2,4-trichlorobenzene (≥99.0%) from Fluka and 2-chlorotoluene (99%) from Aldrich.

Details on NMR spectroscopy are given in the ESI.

Analytical Size Exclusion Chromatography (SEC) was performed using a Spectra series P100

(Spectra Physics) pump equipped with two mixed-B columns (10 μm, 2 × 30 cm, Polymer Labs) and a Refractive Index detector (Shodex) at 60°C. Chlorobenzene was used as the eluent at a flow rate of 1.0 mL min^{-1}. Molecular weight distributions are given relative to polystyrene standards.

UV-Vis was performed on a Varian Cary 500 Scan UV-Vis-NIR spectrophotometer using a data interval of 1 nm, a spectral band width of 2 nm and 0.1 sec signal averaging time. For recording of the absorption maxima in $CHCl_3$ and/or 1,2,4-trichlorobenzene the polymers were dissolved at temperatures that ensured complete dissolution (clear orange solution), quickly cooled to room temperature and measured. P33T for example, was dissolved in 1,2,4-trichlorobenzene at 200 °C (clear orange solution).

Fibre preparation and isolation

Fibre preparation was done under N_2 atmosphere and protected from light. A mixture of polymer in the appropriate solvent was heated for 30 min at temperature T_0 (Table 5) to dissolve the polymer. The orange solution was slowly cooled to room temperature. By simply switching off the heating, the temperature decreased exponentially from T_0 to r.t., typically with half-value decay times with respect to (T_0 – r.t.) of 20 to 60 minutes. The gel that formed was allowed to stand at room temperature for at least 14 h (P33T), 2 days (P34T to P36T) or 10 days (P37T to P39T) before using. After these times, no changes in the UV-Vis were detected and fibre formation was found to be complete. Fibres were isolated by centrifugation for 30 min at 10.000 G (12.000 for P34T in *o*-chlorotoluene).

Table 5 Experimental conditions for P3*A*T fibre preparation. Concentrations are given in Table 2.

A	solvent	T_0 / °C	*t*
3	1,2,4-trichlorobenzene	140	14 h
4	tetralin	100	4 d
4	*o*-chlorotoluene	90	>2 d
5	*p*-xylene	80	2 d
6	*p*-xylene	70	2 d
7	cis/*trans*-decalin	50	2 d
7	pinane	70	2 d
8	pinane	70	7 d
9	pinane	60	12 d

Fibre characterization

AFM measurements were performed in air using a Veeco Dimension microscope equipped with the Nanoscope III controller and the Quadrex module. The scanning process operated in non-contact mode (tapping mode) to avoid tip induced artifacts. Etched Si probe from Nanosensor GmbH (Ref. PPP-NCHR) finally ensures measurements with high spatial resolution (5-10 nm tip radius).

X-ray diffraction (XRD) diffractograms of fibre films were recorded at 20 °C using a Siemens D5000 diffractometer using $CuK_{\alpha 1}$ (1.54056 Å) radiation. The 2θ range measured is 2–40° with a step size of 0.04° and a counting time of 20 s. The films were obtained by drop casting of ~0.3 to 1 wt % solutions (stirred for 24 h) on an SiO_x covered monocrystalline Si(100) substrate, followed by drying in a glove box.

For the TEM measurements freestanding films were prepared. The TEM experiments were performed with a Philips CM12-STEM using an accelerating voltage of 120 kV. Thin films for TEM were prepared by spin coating of a ~ 0.3 to 1 wt % fibre solution (agitated for 24 h) on a glass substrate at 500—2500 rpm (speed depending on viscosity), followed by drying in a glove box when necessary. The polymer films were detached from the glass using a 40% HF solution (*caution*: HF is strongly toxic!) and then washed with distilled water twice.

Differential scanning calorimetry was performed on a TA Instruments DSC 2920 Modulated DSC using aluminium pans and a heating rate of 20° min^{-1}.

Acknowledgements

We thank Guy Reggers for performing DSC measurements, Christel Willems for experimental assistance and both Koen van Vinckenroye and Jos Kaelen for technical assistance. We are also indebted to Sabine Bertho for help with the analysis of the TEM results.

Author contributions

W.D.O. designed and performed experiments, analyzed data and wrote the paper; V.V. performed experiments; S.B. designed experiments and helped in the initial stage of the research; S.G. supervised S.B.; O.D. performed AFM and analyzed the data; B.R. performed XRD; J.D'H. supervised B.R., analysed XRD data, performed TEM and analysed results; P.A. is coordinator of NMR spectroscopy. Performed part of the NMR experiments and analysis; J.M. proposed a matrix of experiments of complementary morphological analysis (AFM, XRD, TEM); L.L. initiated the research and supervised W.D.O.; D.V. supervised W.D.O.

Literature

1. K. J. Ihn, J. Moulton and P. Smith, *J. Polym. Sci., Part B: Polym. Phys.*, 1993, **31**, 735-742.
2. J.-F. Chang, J. Clark, N. Zhao, H. Sirringhaus, D. W. Breiby, J. W. Andreasen, M. M. Nielsen, M. Giles, M. Heeney and I. McCulloch, *Phys. Rev. B: Condens. Matter*, 2006, **74**, 115318.
3. S. Berson, R. De Bettignies, S. Bailly and S. Guillerez, *Adv. Funct. Mater.*, 2007, **17**, 1377-1384.
4. X. Yang, J. Loos, S. C. Veenstra, W. J. H. Verhees, M. M. Wienk, J. M. Kroon, M. A. J. Michels and R. A. J. Janssen, *Nano Lett.*, 2005, **5**, 579-583.
5. M. Surin, P. Leclère, R. Lazzaroni, J. D. Yuen, G. Wang, D. Moses, A. J. Heeger, S. Cho and K. Lee, *J. Appl. Phys.*, 2006, **100**, 033712.
6. J. M. Verilhac, G. LeBlevennec, D. Djurado, F. Rieutord, M. Chouiki, J. P. Travers and A.

Pron, *Synth. Met.*, 2006, **156**, 815-823.
7. G. Li, Y. Yao, H. Yang, V. Shrotriya, G. Yang and Y. Yang, *Adv. Funct. Mater.*, 2007, **17**, 1636-1644.
8. Z. Bao, A. Dodabalapur and A. J. Lovinger, *Appl. Phys. Lett.*, 1996, **69**, 4108-4110.
9. J.-F. Chang, B. Sun, D. W. Breiby, M. M. Nielsen, T. I. Sölling, M. Giles, I. McCulloch and H. Sirringhaus, *Chem. Mater.*, 2004, **16**, 4772-4776.
10. Y. Zhao, G. Yuan and P. Roche, *Polymer*, 1995, **36**, 2211-2214.
11. A. Swinnen, I. Haeldermans, P. Vanlaeke, J. D'Haen, J. Poortmans, M. D'Olieslager and J. V. Manca, *Eur. Phys. J. Appl. Phys.*, 2007, **36**, 251-256.
12. S. Miller, G. Fanchini, Y. Y. Lin, C. Li, C. W. Chen, W. F. Su and M. Chhowalla, *J. Mater. Chem.*, 2008, **18**, 306-312.
13. J. A. Merlo and C. D. Frisbie, *J. Polym. Sci., Part B: Polym. Phys.*, 2003, **41**, 2674-2680.
14. J. A. Merlo and C. D. Frisbie, *J. Phys. Chem. B*, 2004, **108**, 19169-19179.
15. S. Cho, K. Lee, J. Yuen, G. Wang, D. Moses, A. J. Heeger, M. Surin and R. Lazzaroni, *J. Appl. Phys.*, 2006, **100**, 114503.
16. A. J. Moulé and K. Meerholz, *Adv. Mater.*, 2008, **20**, 240-245.
17. H. Xin, F. S. Kim and S. A. Jenekhe, *J. Am. Chem. Soc.*, 2008, **130**, 5424-5425.
18. H. Xin, G. Ren, F. S. Kim and S. A. Jenekhe, *Chem. Mater.*, 2008, **20**, 6199-6207.
19. S. Allard, M. Forster, B. Souharce, H. Thiem and U. Scherf, *Angew. Chem. Int. Ed.*, 2008, **47**, 4070-4098.
20. L. Li, G. Lu and X. Yang, *J. Mater. Chem.*, 2008, **18**, 1984-1990.
21. S. Samitsu, T. Shimomura and K. Ito, *Thin Solid Films*, 2008, **516**, 2478-2486.
22. S. Samitsu, T. Shimomura, S. Heike, T. Hashizume and K. Ito, *Macromolecules*, 2008, **41**, 8000-8010.
23. R. Zhang, B. Li, M. C. Iovu, M. Jeffries-EL, G. Sauvé, J. Cooper, S. Jia, S. Tristam-Nagle, D. M. Smilgies, D. N. Lambeth, R. D. McCullough and T. Kowalewski, *J. Am. Chem. Soc.*, 2006, **128**, 3480-3481.
24. J. S. Liu, R. S. Loewe and R. D. McCullough, *Macromolecules*, 1999, **32**, 5777-5785.
25. S. Holdcroft, *J. Polym. Sci., Part B: Polym. Phys.*, 1991, **29**, 1585-1588.
26. E. J. Samuelsen and J. Mårdalen, in *Handbook of Organic Conductive Molecules and Polymers*, ed. H. S. Nalwa, John Wiley & Sons Ltd, Chichester, 1997, pp. 87-120.
27. T. A. Chen, X. M. Wu and R. D. Rieke, *J. Am. Chem. Soc.*, 1995, **117**, 233-244.
28. R. D. McCullough, *Adv. Mater.*, 1998, **10**, 93-116.
29. A. Zen, M. Saphiannikova, D. Neher, U. Asawapirom and U. Scherf, *Chem. Mater.*, 2005, **17**, 781-786.
30. A. F. M. Barton, *CRC Handbook of Solubility Parameters and Other Cohesion Parameters*, CRC Press, Boca Raton, 1991.
31. C. M. Hansen, *Hansen solubility parameters: a user's handbook*, CRC Press, Boca Raton, 2000.
32. D. M. Koenhen and C. A. Smolders, *J. Appl. Polym. Sci.*, 1975, **19**, 1163-1179.
33. W. Zeng, Y. Du, Y. Xue and H. L. Frisch, in *Physical Properties of Polymers Handbook*, ed. J. E. Mark, Springer Science+Business Media, New York, 2007, pp. 289-303.
34. Note that Hansen parameters for 1,2,4-trichlorobenzene, o-chlorotoluene, 1,2,4-trimethylbenzene, o-xylene and pinane were not available. Of the remaining solvents, anisol and cyclohexanone have dH [dP] values of 6.8 [4.1] and 5.1 [6.3] MPa1/2, respectively, versus values of 0 to 3.3 [6.3] for the other solvents.
35. D. R. Lide, ed., *CRC Handbook of Chemistry and Physics*, CRC Press, Boca Raton, 1992.
36. S. Malik and A. K. Nandi, *J. Appl. Polym. Sci.*, 2007, **103**, 2528-2537.
37. Note that log MW has a virtually linear dependence on elution time t for our instrument in the MW region of interest, and hence no noticeable error is introduced by taking log MW instead of t.
38. T. J. Prosa, M. J. Winokur, J. Moulton, P. Smith and A. J. Heeger, *Macromolecules*, 1992, **25**, 4364-4372.
39. T. J. Prosa, M. J. Winokur and R. D. McCullough, *Macromolecules*, 1996, **29**, 3654-3656.

40. S. V. Meille, V. Romita, T. Caronna, A. J. Lovinger, M. Catellani and L. Belobrzeckaja, *Macromolecules*, 1997, **30**, 7898-7905.
41. K. Tashiro, Y. Minagawaa, M. Kobayashia, S. Moritab, T. Kawaib and K. Yoshino, *Synth. Met.*, 1993, **55**, 321-328.
42. T. Yamamoto, D. Komarudin, M. Arai, B. L. Lee, H. Suganuma, N. Asakawa, Y. Inoue, K. Kubota, S. Sasaki, T. Fukuda and H. Matsuda, *J. Am. Chem. Soc.*, 1998, **120**, 2047-2058.
43. F. C. Spano, *J. Chem. Phys.*, 2005, **122**, 234701.
44. F. C. Spano, *Chem. Phys.*, 2006, **325**, 22-35.
45. J. Clark, C. Silva, R. H. Friend and F. C. Spano, *Phys. Rev. Lett.*, 2007, **98**, 206406.
46. S. Malik and A. K. Nandi, *J. Phys. Chem. B*, 2004, **108**, 597-604.
47. K. Tamao, S. Kodama, I. Nakajima, M. Kumada, A. Minato and K. Suzuki, *Tetrahedron*, 1982, **38**, 3347-3354.
48. P. Bauerle, F. Pfau, H. Schlupp, F. Wurthner, K. U. Gaudl, M. B. Caro and P. Fischer, *J. Chem. Soc., Perkin Trans. 2*, 1993, 489-494.
49. T. A. Chen and R. D. Rieke, *J. Am. Chem. Soc.*, 1992, **114**, 10087-10088.

Supplementary Information

Poly(3-alkylthiophene) synthesis

A short description of the synthesis of P36T is given. Other polymers were synthesized in an identical way, starting with different alkyl Grignard reagents.

Hexylmagnesium bromide (Aldrich, 2M in diethyl ether) was coupled to 3-bromothiophene (ACROS, 97%) in dry diethyl ether at room temperature using Ni(dppp)Cl_2 as the catalyst following published procedures.[47] The resulting 3-hexylthiophene was purified by vacuum distillation and converted into 2,5-dibromo-3-hexylthiophene in DMF using 2.2 eq. of NBS following Bäuerle *et al.*[48] The resulting product was purified by vacuum distillation.

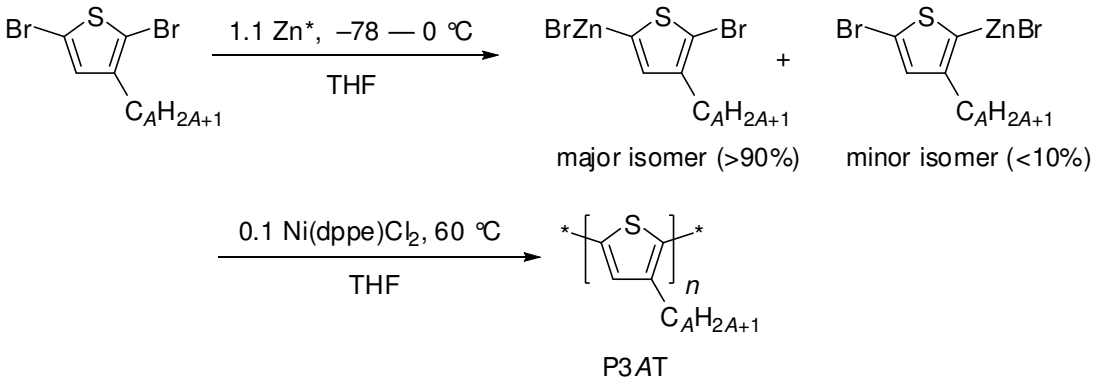

SI_Figure 1. Synthesis of poly(3-alkylthiophene)s (P3*A*T) *via* the Rieke method.

Poly(3-hexylthiophene) was prepared by reacting 2,5-dibromo-3-hexylthiophene with Rieke Zn*, followed by polymerisation with Ni(dppe)Cl_2 (0.1 eq) in THF at 60 °C according to literature procedures.[27, 49] The polymers were purified by precipitation in 2 M HCl—MeOH (1 : 2), followed by filtration and Soxhlet extraction with MeOH (24 h) and hexane (24 h). Yields varied from 50 % (P39T) to 66–80% (P33T to P38T). The polymers were characterized by ^{1}H- and ^{13}C-NMR, FT-IR and GPC. Analytical data were found to be in agreement with literature.[27] The ^{1}H- and ^{13}C-NMR data follow below:

Poly(3-propylthiophene) (P33T) ^{1}H-NMR (1,4-dichlorobenzene-d_4 @ 120 °C): δ 1.00 (t, J = 7.2 Hz, 3H), 1.75 (tt, J ~ 7.4 Hz, 2H), 2.81 (t, J = 7.5 Hz), 7.04 (s, 1H). ^{13}C-NMR (1,4-dichlorobenzene-d_4 @ 120 °C): δ 13.9, 23.8, 31.8, 129.0, 131.3, 134.4, 140.0.

Poly(3-butylthiophene) (P34T) ^{1}H-NMR (CS_2 with some drops of $CDCl_3$ @ 20 °C): δ 1.00—1.06 (m, 3H), 1.46—1.55 (m, 2H), 1.65—1.75 (m, 2H), 2.53—2.62 (m, 0.07H), 2.76—2.81 (m, 1.93H), 6.89 (s, 1H). *RR* 96.5%; ^{13}C-NMR (CS_2 with some drops of $CDCl_3$) δ 14.2, 23.0, 29.2, 32.7, 128.3, 130.4, 133.5, 139.2.

Poly(3-pentylthiophene) (P35T) ^{1}H-NMR: δ 0.90—0.95 (m, 3H), 1.35—1.45 (m, 4H), 1.66—1.76 (m, 2H), 2.54—2.61 (m, 0.11H), 2.77—2.82 (m, 1.89H), 6.97 (s, 1H). ^{13}C-NMR: δ 14.0, 22.5, 29.5, 30.2, 31.8, 128.7, 130.7, 133.9, 140.0.

Poly(3-hexylthiophene) (P36T) ^{1}H-NMR: δ 0.88—0.93 (m, 3H), 1.26—1.46 (m, 6H), 1.65—1.75 (m, 2H), 2.54—2.59 (m, 0.10H), 2.77—2.82 (m, 1.90H), 6.97 (s, 1H). ^{13}C-NMR: δ 14.0, 22.6, 29.2, 29.5, 30.5, 31.7, 128.7, 130.7, 133.9, 140.0.

Poly(3-heptylthiophene) (P37T) ^{1}H-NMR: δ 0.87—0.91 (m, 3H), (1.31—1.45, 8H), 1.65—1.75 (m, 2H), (2.54—2.59, 0.06H), 2.80 (br m, 1.94H), 6.95 (s, 1H). ^{13}C-NMR: δ 14.0, 22.7, 29.2 (2x), 29.6, 30.6, 31.9, 128.7, 130.7, 133.9, 140.0.

Poly(3-octylthiophene) (P38T) ^{1}H-NMR: δ 0.86—0.90 (m, 3H), 1.29—1.45 (m, 10H), 1.65—1.75 (m, 2H), 2.54—2.59 (m, 0.07H), 2.80 (br m, 1.93H), 6.95 (s, 1H). ^{13}C-NMR: δ 14.0, 22.7, 29.3, 29.5, 29.6, 29.7, 30.6, 31.9, 128.7, 130.7, 133.9, 140.0.

Poly(3-nonylthiophene) (P39T) ^{1}H-NMR: δ 0.85—0.92 (m, 3H), 1.28—1.45 (m, 12H), 1.65—1.75 (m, 2H), 2.54—2.59 (m, 0.04H), 2.81 (br m, 1.96H), 6.93 (br s, 1H). ^{13}C-NMR: δ 14.0, 22.7, 29.3, 29.5—29.6 (3 overlapping signals), 29.7, 30.6, 31.9, 128.7, 130.7, 133.9, 140.0.

NMR spectroscopy

NMR spectra were recorded in $CDCl_3$ at 50 °C on a Varian Inova 300 spectrometer at 299.808 MHz for ^{1}H and at 75.394 MHz for ^{13}C using 5 mm probes, unless stated otherwise. ^{1}H and ^{13}C chemical shifts are reported in ppm downfield from tetramethylsilane (TMS) reference using the residual C-*H* solvent resonance (^{1}H-NMR) and the *C*-D resonance (^{13}C-NMR) as an internal standard. For $CDCl_3$ these were set at 7.24 ppm and 77.00 ppm, respectively. For 1,4-dichlorobenzene-d_4 at 120 °C they were set at the values that we measure with respect to TMS at 60 °C; 7.03 ppm and 129.4 ppm, respectively. In CS_2 containing $CDCl_3$ (used for P34T), the shifts were referenced to $CDCl_3$ with the above-mentioned reference values.

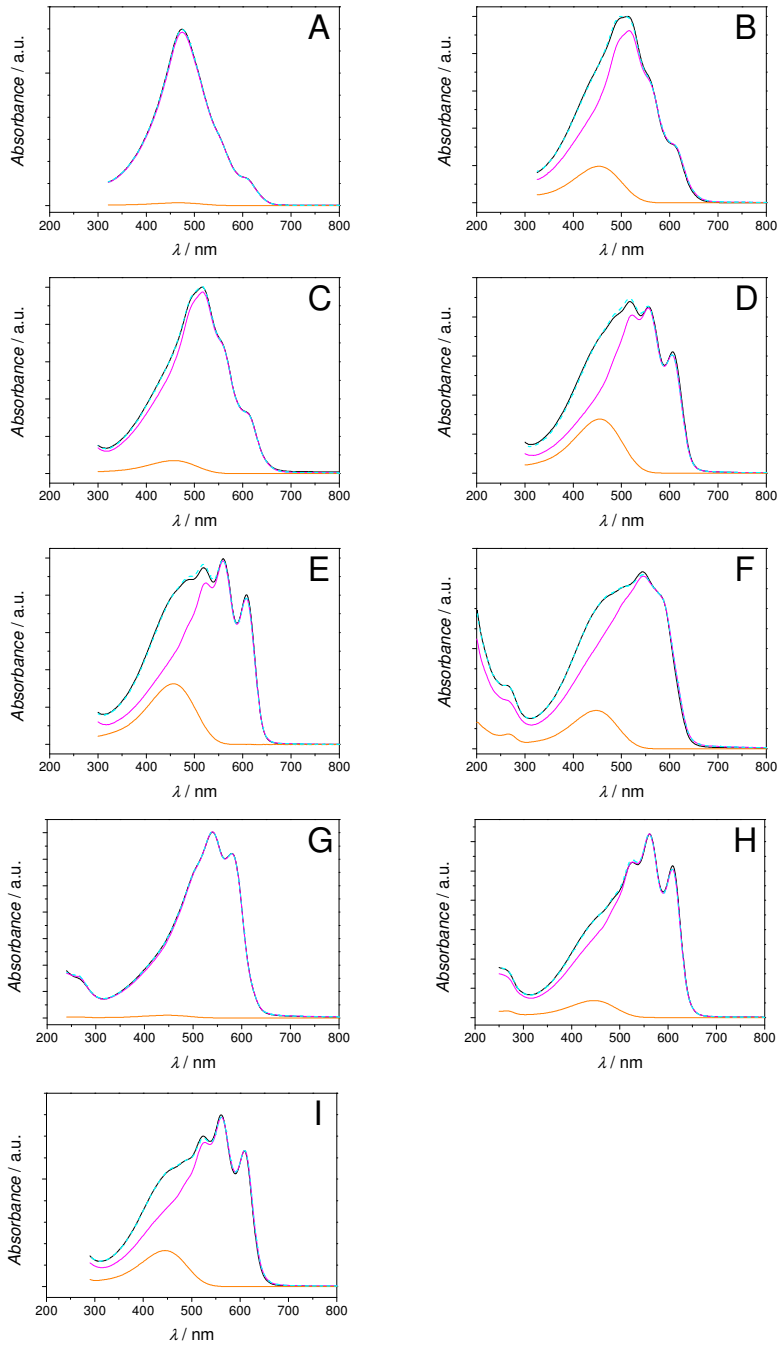

SI_Figure 2 UV-Vis absorption spectra of pristine fibre solutions of P33T—P39T in various solvents (black line) together with the fit results (blue dash) of fitting them as a sum of the pure fibre (purple line) and `amorphous´ (orange line) spectra. A) P33T in 1,2,4-trichlorobenzene; B) P34T in tetralin; C) P34T in *o*-chlorotoluene; D) P35T in *p*-xylene; E) P36T in *p*-xylene; F) P37T in *cis*/*trans*-decalin; G) P37T in Pinane; H) P38T in Pinane; I) P39T in Pinane.

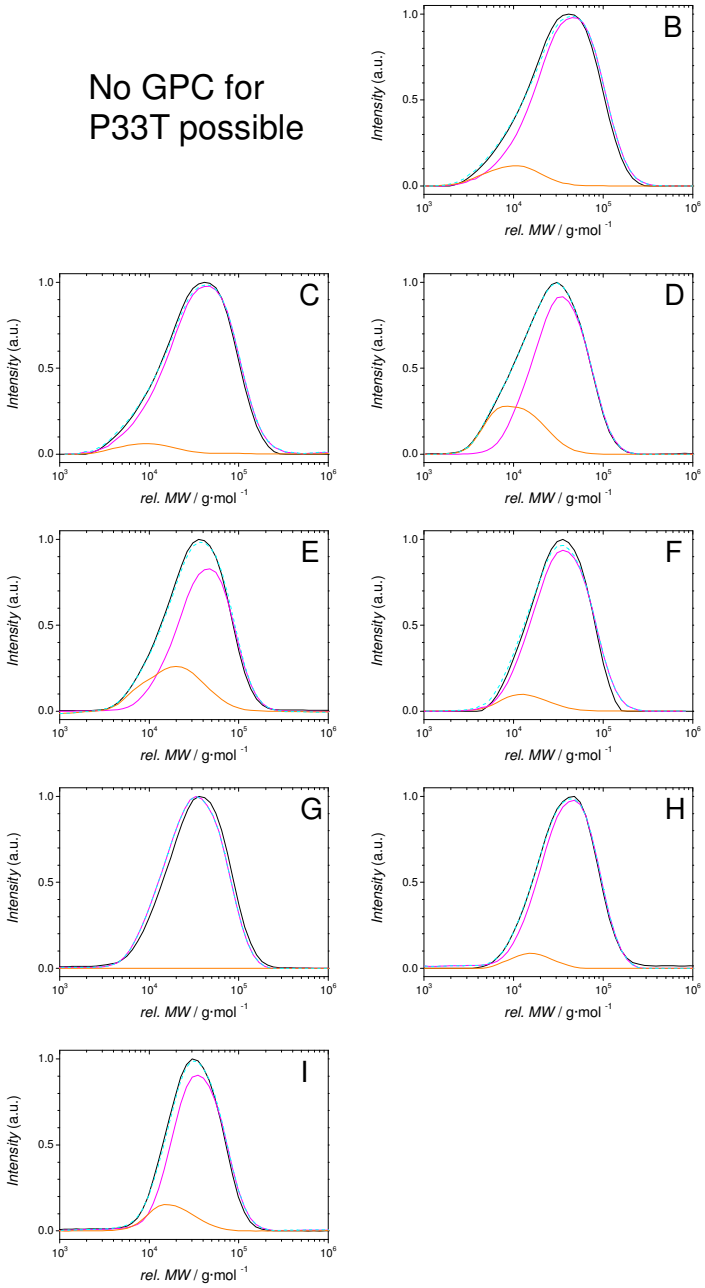

SI_Figure 3 GPC curves of P3ATs **P34T—P39T** in chlorobenzene at 60 °C versus polystyrene standards (black line) together with the fit results (blue dash) of fitting them as a sum of GPC curves of the isolated fibre (purple line) and `amorphous´ (orange line) fractions. For letter-coding, see **SI_Figure 2**.

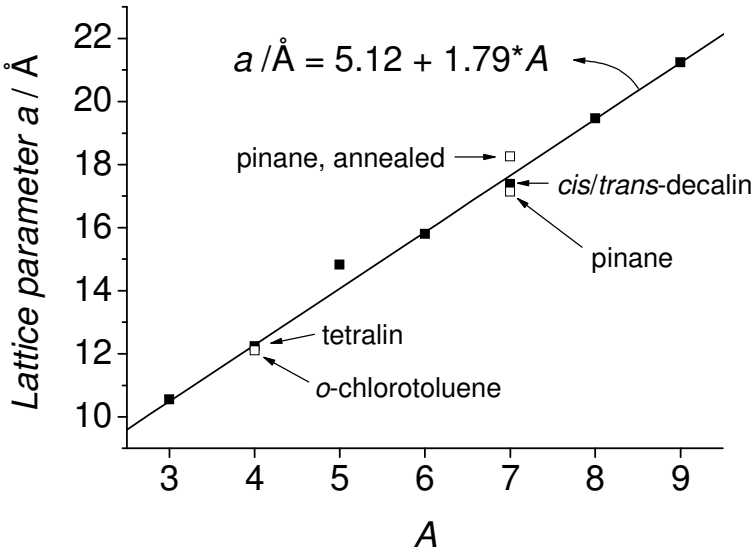

SI_Figure 4 Lattice parameter *a* for isolated fibres from XRD as a function of alkyl chain length *A*. together with a linear fit through the data (except P35T and P37T).

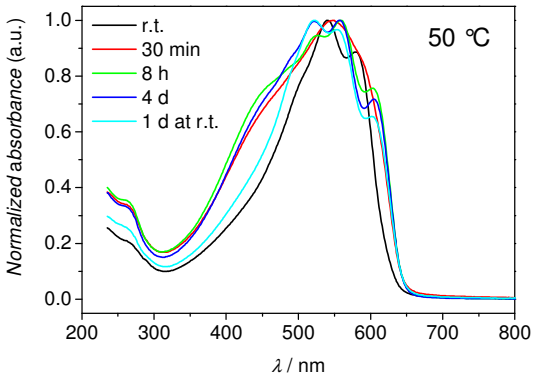

SI_Figure 5 Time evolution of the UV-Vis spectrum of 0.5 wt. % P37T fibres in pinane at 50 °C. Shown spectra were taken at room temperature, after 30 min, 8 h and after 4 days, when the solution was cooled to r.t. The last spectrum was taken 24 h after cooling to r.t.